Available free online at www.medjchem.com

Mediterranean Journal of Chemistry

Mediterranean Journal of Chemistry **2019**, 9(3), 199-211

Structural, electronic, optical properties and first-principles calculations of $Sr_{1-x}Ca_xWO_4$ ceramics

Mohammed Ait Haddouch [1,*], Youssef Tamraoui [2,*], Fatima Ezzahra Mirinioui [3], Youssef Aharbil [1], Hicham Labrim [4], Bouchaib Manoun[2,3], Abdelilah Benyoussef [5] and Said Benmokhtar [1]

[1] Laboratoire de Chimie Physique des Matériaux LCPM, Faculté des Sciences Ben M'Sik, Casablanca, Morocco

[2] Materials Science and Nano-engineering Department, Mohammed VI Polytechnic University, Ben Guerir, Morocco

[3] Université Hassan 1er, laboratoire des Sciences des Matériaux, des Milieux et de la modélisation (LS3M),25000, Khouribga, Morocco

[4] Centre National de l'Energie, des Sciences et des Techniques Nucléaires, Rabat, Morocco

[5] Laboratoire de Magnétisme et Physique des Hautes Energies L.M.P.H.E. URAC 12, Université Mohammed V, Faculté des Sciences, B.P. 1014, Rabat, Morocco

Abstract: A series of strontium calcium tungstates $Sr_{1-x}Ca_xWO_4$ powders with (x = 0; 0.25; 0.5; 0.75 and 1.0) were prepared by solid-state reaction method and analyzed by X-ray diffraction (XRD). All these compositions possess a tetragonal scheelite structure with $I4_1/a$ space group. Raman active vibrational modes in the range from 20 to 1000 cm^{-1} of the series $Sr_{1-x}Ca_xWO_4$ with tetragonal structure exhibit 13 modes in arrangement with the Group theory analysis of structural Raman-active modes. The optical properties were investigated using the diffuse reflectance UV–visible absorbance spectrum. Based on Density Functional Theory (DFT) and using full Potential-linearized Augmented Plane Wave (FP-LAPW) method with the Local Density Approximation and the Generalized Gradient Approximation (GGA), implemented in the Wien2k package, we have investigated electronic and optical properties of all the compositions. The results indicate a decrease in the values of the optical direct bandgap (from 4.29 to 3.87 eV) with the increase of Ca into $SrWO_4$ lattice, which is in good agreement with our experimental results.

Keywords: $Sr_{1-x}Ca_xWO_4$; Rietveld refinement; Raman spectroscopy; DFT; Optical properties; Wien2K; band structure.

1. Introduction

At ambient conditions, alkaline-earth-metal-tungstates AWO_4 (A=Ca, Sr, Ba, Pb) with the tetragonal scheelite structure [1], represent an essential family of inorganic wide bandgap semiconductors [2]. The divalent A^{2+} and hexavalent W^{6+} atoms surrounded by eight and four O^{2-} atoms, respectively. These materials have vast applications in various fields such as electro-optics, lasers, and amplifiers [3] due to their excellent properties as scintillating crystals. Recently, the bandgap energy (Eg) values of similar material types have been reported and it has been revealed to be susceptible to the ionic radii and the electronic configuration of alkaline-earth-metal [2,4].

Scheelite materials drew the interest of crystal growers, material scientists and physicists due to their potential application in the optoelectronic industries. Calcium tungstate is abundantly used phosphor in industrial and medical applications [5].

Several synthesis techniques have been employed for the preparation of AWO_4 (A= Ca, Sr, and Ba) compounds, such as electrochemical [6,7], high-temperature flux crystallization [8], hydrothermal-electrochemical [9], polymeric precursor [10] and molten salt [11]. The expensive precursors used in these methods and their high consumption of electric energy [12] make the solid-state reaction [13] used in this work an ideal choice because of its cost-effectiveness [14].

Q. Guo et al. [15] investigate the thermodynamic properties of AWO_4 (A = Mg, Ca, Sr, Ba) and reported that SrWO4 is more stable thermodynamically than $CaWO_4$. The optical properties of $CaWO_4$ and $SrWO_4$ were reported in refs [2,16] using UV–vis spectroscopies technique.

**Corresponding authors: Mohammed Ait Haddouch; Youssef Tamraoui*
Electronic mail:mohammed.ait.haddouch@gmail.com, youssef.tamraoui@um6p.ma
DOI: http://dx.doi.org/10.13171/mjc93191005355mah/yt

Received July 5, 2019
Accepted August 31, 2019
Published October 5, 2019

Thus, in this report, we aim to explore the correlation between the variation in the chemical composition of $Sr_{1-x}Ca_xWO_4$ (0≤x≤1) scheelite material and its electronic structure properties. Consequently, the main goal is to investigate the crystal structure and optical properties using X-ray diffraction and UV-Visible measurements of the prepared $Sr_{1-x}Ca_xWO_4$ using the solid-state reaction technique. Also, calculate its electronic structure and optical properties by applying density functional theory (DFT) and using all-electron full-potential linearized augmented plane wave (FP-LAPW) method [17].

2. Methods

2.1. Samples preparation

Powders of the $Sr_{1-x}Ca_xWO_4$ system with (0≤x≤1) were prepared by the solid-state reaction from stoichiometric amounts of WO_3 (99.9%) with metal carbonate ($BaCO_3$ 99.98%, $SrCO_3$ 99.9%). The samples were heated in air, in alumina crucibles, at progressively higher temperatures (600°C/24h, 800°C/24 h, and 1000°C/24 h) with periodic intermediate regrinding. The chemical reaction is:

$$\mathbf{(1-x)SrCO_3 + xCaCO_3 + WO_3 \rightarrow Sr_{1-x}Ca_xWO_4 + CO_2\uparrow.}$$

The final products of these series have been controlled by X-ray powder diffraction analysis using CuKα radiation.

2.2. XRD measurements

Diffraction data were collected at room temperature on a D2 PHASER diffractometer, with the Bragg-Brentano geometry (θ-θ), using CuKα radiation (λ = 1.5418 Å) with 30 kV and 10 mA. The XRD patterns were scanned through 2θ range 15–80° with a step size of 0.01°.

The Rietveld refinements were carried out using Fullprof program [18] integrated into Winplotr software [19].

We initiated the observed powder XRD data with scale and background parameters and in order, other profile parameters are included. Pseudo-Voigt profile function for peak shape fitting. The position parameters and isotropic atomic displacement parameters of individual atoms were also refined after an appreciable profile matching.

2.3. Raman spectroscopy

Vibrational studies were performed using a Raman spectrometer designed and built at the Department of Earth Sciences, Uppsala University [20]. Details of Raman spectroscopy experiment procedures are found elsewhere [21]. Raman spectra have been analyzed, with the peak-fitting function in origin software [22]. A'Gauss/Lorentz' function was chosen for peak profiles, and Savitzky-Golay algorithm was used as a data smoothing method. The background intensity was subtracted before fitting, and the fitting process proceeded until minimum residuals were reached.

2.4. Optical measurements

In general Solid UV-vis spectroscopy investigation, on powder materials uses small sample quantities. In the present study, powder samples were filled into a cylindrical sample holder with a surface of 1.5 square centimeters, and 1.0 mm thickness layer. The optical absorption experiments were carried out by PerkinElmer LAMBDA™ 1050 UV/Vis/NIR spectrometer, equipped with an integrating sphere in the range of 250-1800 nm with a 1 nm interval, in order to accurately determine the optical absorption edge in near UV. The spectra were converted from reflectance to absorbance by using the computer program UV WinLab DPV which is based on solving the Kubelka–Munk function [23]. The optical band gap energy was then estimated using the onset of the absorption edge by Tauc plots [24].

2.5. Computational Methods

We Obtained the structure file used for the theoretical calculations from Rietveld refinement of X-ray powder diffraction data obtained for all $Sr_{1-x}Ca_xWO_4$ stoichiometric compositions in our experimental study, in order to compute the optical properties presented in this work.

The band structure and density of states (DOS) calculations including optical properties are done using full-potential linearized augmented plane wave (FP-LAPW) based on density functional theory (DFT) [17] as implemented in Wien2k [25]. Moreover, the exchange-correlation potential was calculated using the generalized gradient approximation (GGA) formulated by Perdew, Burke, and Ernzerhof (PBE) [26]. The precise input of energy eigenvalues and energy eigenfunction to calculate optical properties were obtained from the band structure calculations. The charge density was Fourier expanded up to G_{max} = 12(a.u.$^{-1}$). The cutoff energy is considered to be -6 Ryd. 35 k-points in a grid of 10×10×10 has been used for reciprocal space integration in the irreducible Brillouin zone (BZ), to achieve self-consistency. In the optical properties calculations, we used 1000 K-points in the entire BZ. The convergence criteria for the self-consistent calculation for stability were taken to be 10^{-6} Ryd.

3. Results and discussion

3.1. Crystal structure investigation

Fig. 1(A) shows the X-ray powder diffraction patterns of $Sr_{1-x}Ca_xWO_4$. Dicvol program [27] was used for indexing of the X-ray powder diffraction patterns of all compositions. All diffraction peaks show a single-phase tetragonal structure (scheelite type) with space group $I4_1/a$. The diffraction patterns of all compositions present crystalline nature. No additional or intermediate phases were detected. Due to the

smaller ionic radius of Ca^{2+} (1.12 Å) compared to Sr^{2+} (1.26 Å) [28], there is a gradual increase in the shift of 2θ position as substituting Sr^{2+} by Ca^{2+}. The lattice parameters that were refined using the complete powder diffraction data sets are listed in Table 1. The variation of the unit cell volume in the studied composition range in $Sr_{1-x}Ca_xWO_4$ ($0 \le x \le 1$) is shown in Fig. 1(B). As can be seen, there is a gradual decrease in the unit cell parameters as with the amount of Ca^{2+} increases, consistent with the lower ionic radius of Ca^{2+} (1.12 Å) compared to Sr^{2+} (1.26 Å). These values for x=0 and x=1 agreed well with those reported in the literature [13,29]. The obtained lattice parameters are also in good agreement with JCPDS card no 85-0587 for $SrWO_4$ and 77- 2237 for $CaWO_4$.

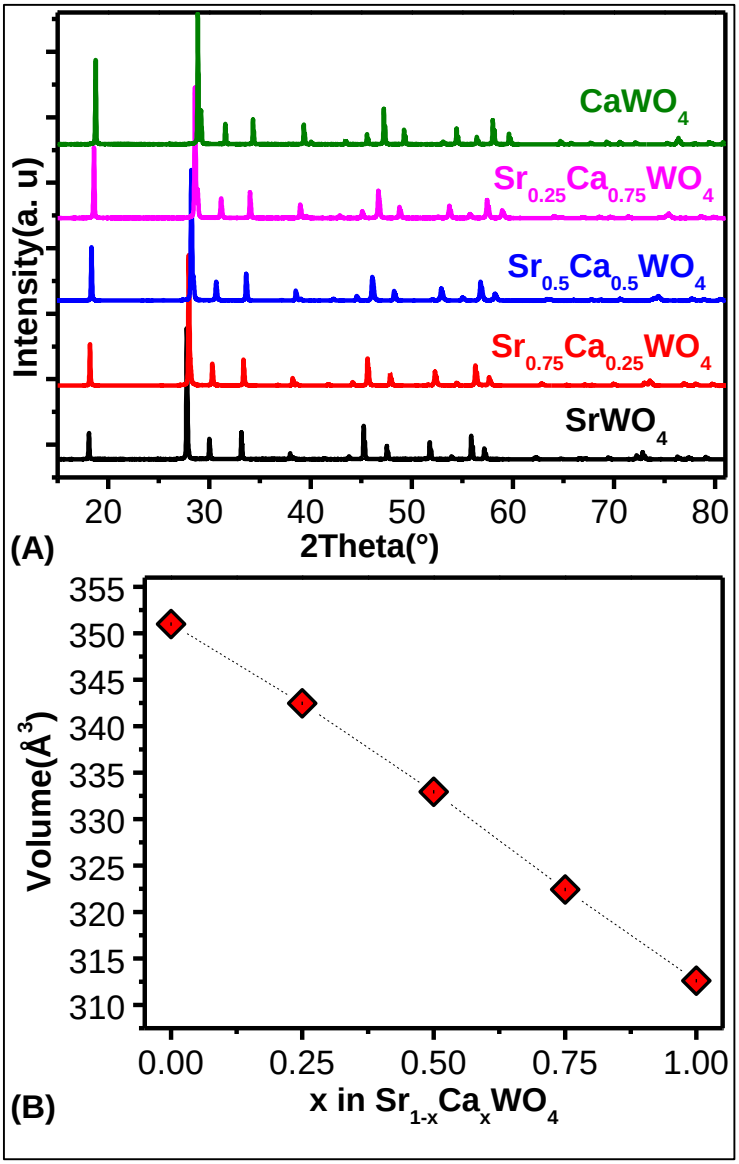

Figure. 1. (A): Illustration of the X-ray diffraction patterns of $Sr_{1-x}Ca_xWO_4$ ceramics, (B): variation of the unit cell volume of $Sr_{1-x}Ca_xWO_4$ as a function of Ca amount.

The X-ray powder patterns were fitted to the calculated ones using a full-profile analysis program [18,19] to minimize the profile discrepancy factor Rp. For $Sr_{1-x}Ca_xWO_4$ ($0 \le x \le 1$), the refinement of the powder XRD patterns were carried out with tetragonal ($I4_1/a$) lattice with a starting model taken from Ref [30]. In this model Sr^{2+}/Ca^{2+} and W^{6+} are placed at 4b (0, 1/4, 5/8) and 4a (0, 1/4, 1/8) sites, respectively; the oxygen atoms occupy the 16f Wyckoff positions (x, y, z). As an example, we show, in Fig. 2, the typical Rietveld refinement patterns along with the difference plot at ambient temperature for $Sr_{1-x}Ca_xWO_4$ (x=0.25;0.5;0.75). For all investigated compounds, the refinements of the occupancies of all atoms show no significant deviation from their stoichiometric values. Significantly right residuals of the refinements are obtained with χ^2 factor ≤ 1.45. The refined position coordinates for $Sr_{1-x}Ca_xWO_4$ ($0 \le x \le 1$) in the tetragonal compositions are given in Table 1.

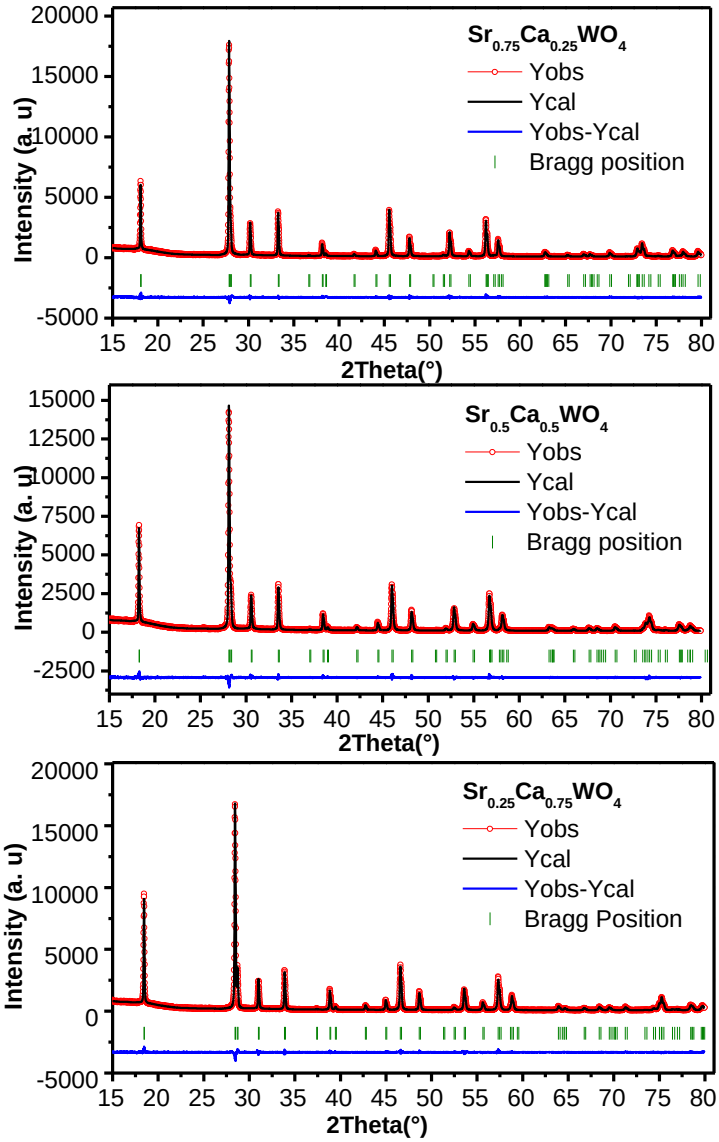

Figure. 2. Rietveld refinement plots for the series $Sr_{1-x}Ca_xWO_4$ for the compositions x=0.25, x=0.5 and x=0.75.

The upper symbols illustrate the observed data (red circles) and the calculated pattern (solid line). The vertical markers show calculated positions of Bragg reflections. The lower curve is the difference diagram.

The analysis of the refined crystallographic parameters in $Sr_{1-x}Ca_xWO_4$ ($0 \leq x \leq 1$) indicates that W^{6+} is coordinated by four oxygen atoms in a tetrahedral configuration with a symmetry group Td. These tetrahedra were slightly distorted in matrix $Sr_{1-x}Ca_xWO_4$ lattice. As a result, this distortion in WO_4-tetrahedra causes changes in W–O bond length (see Table 2) which further modified the energy levels and enhanced structural order-disorder in the host lattice [31]. The relative distortion can be measured by calculating the relative deviation from the average bond length of the polyhedral Δ_{pol} as given by Fleet in 1976 [32]:

$$\Delta_{Tet} = \frac{1}{4}\sum_{i=1}^{4}\left[(d_i - d_0)/d_0\right]^2$$

Where d_0 is the theoretical bond length calculated from the ionic radii taken from Shannon tables [28] and d_i is the bond length obtained from the Rietveld refinement. The relative distortions of WO_4-tetrahedra in $Sr_{1-x}Ca_xWO_4$ are illustrated in Table 2.

Table 1. Details of Rietveld refinement conditions and Refined structural parameters for $Sr_{1-x}Ca_xWO_4$ ($0 \leq x \leq 1$) with $I4_1/a$ as space group.

	$SrWO_4$	$Sr_{0.75}Ca_{0.25}WO_4$	$Sr_{0.5}Ca_{0.5}WO_4$	$Sr_{0.25}Ca_{0.75}WO_4$	$CaWO_4$
a(Å)	5.4184	5.3801	5.3372	5.288	5.2424
c(Å)	11.9555	11.83179	11.68817	11.52847	11.37445
V(Å^3)	351.005	342.480	332.940	322.418	312.603
Sr/Ca	4b (0, ¼ , ⅝)	4b (0, ¼ , ⅝)	4b (0, ¼ , ⅝)	4b (0, ¼ , ⅝)	4b (0, ¼ , ⅝)
Biso(Å^3)	0.767(63)	0.833(63)	0.740(93)	0.999(68)	1.293(85)
W	4a (0, ¼, ⅛)	4a (0, ¼, ⅛)	4a (0, ¼, ⅛)	4a (0, ¼, ⅛)	4a (0, ¼, ⅛)
Biso(Å^3)	0.187(42)	0.136(40)	0.995(55)	0.314(35)	0.238(31)
O	16f (x, y, z)	16f (x, y, z)	16f (x, y, z)	16f (x, y, z)	16f (x, y, z)
X	0.2229(10)	0.2314(10)	0.2358(10)	0.2350(8)	0.2375(8)
Y	0.1109(8)	0.1144(8)	0.1074(10)	0.1029(8)	0.1027(8)
Z	0.0457(4)	0.0449(4)	0.0466(4)	0.0426(3)	0.0411(4)
Biso(Å^3)	2.146(23)	2.409(251)	3.693(356)	2.662(203)	1.731(189)
R_f, R_B	1.1, 1.142	1.558, 2.281	1.386, 2.677	1.289, 2.323	1.290, 2.445
Rp, Rwp	8.68, 9.97	10.2, 10.4	10.6, 10.5	9.38, 9.74	10.9, 10.5
χ2	1.33	1.42	1.45	1.40	1.42
U	0.02932 (6)	0.05873 (6)	0.08924 (6)	0.07890 (5)	0.03012 (6)
V	-0.01879 (6)	-0.01313 (6)	-0.00625 (6)	-0.01232 (6)	-0.01491 (6)
W	0.00777 (6)	0.00950 (5)	0.01101 (6)	0.008250 (15)	0. 0.00741 (6)
Zero (°2θ)	-0.01194(5)	0.0353(4)	0.0720 (9)	0.0164 (4)	0.0529 (4)

Table 2. Selected interatomic distances (Å), and relative distortions of WO_4-tetrahedra in the series $Sr_{1-x}Ca_xWO_4$ ($0 \leq x \leq 1$).

Composition	X=0	X=0.25	X=0.5	X=0.75	X=1
8×Sr/Ca-O	4×2.641 (5)	4×2.614(5)	4×2.543(5)	4×2.520(4)	4×2.495(4)
	4×2.643 (5)	4×2.581(5)	4×2.567(5)	4×2.511(4)	4×2.462(4)
<Sr/Ca-O>	2.64235	2.59725	2.55505	2.51515	2.4781
4×<W-O>	1.710(5)	1.726(5)	1.733(5)	1.747(4)	1.749(4)
Δ_{Tet} in 4a site (WO_4)	3.63×10^{-3}	2.64×10^{-3}	2.30×10^{-3}	1.61×10^{-3}	1.54×10^{-3}

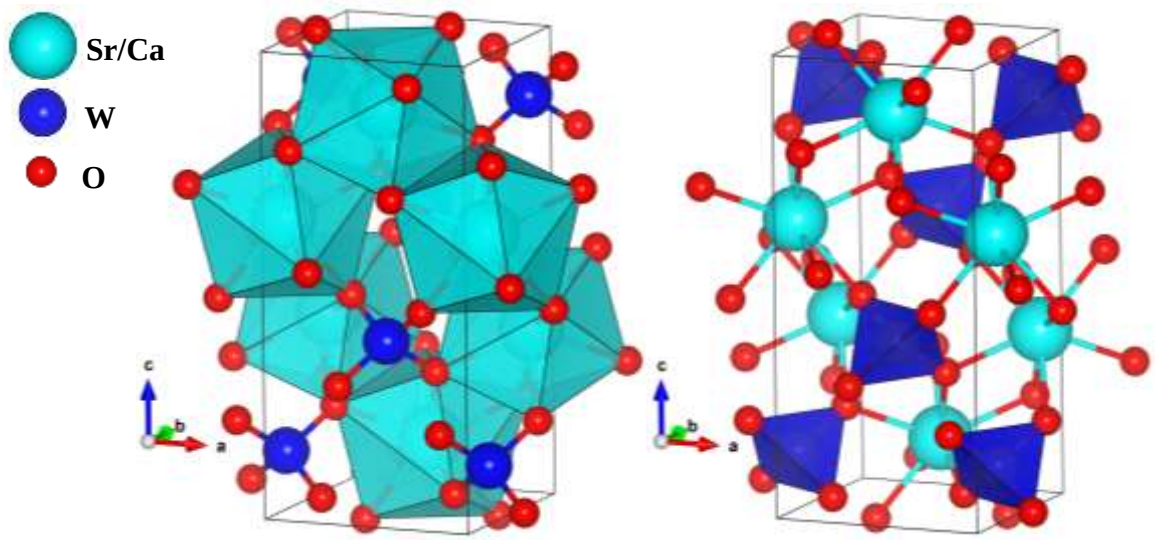

Figure. 3. Schematic representation of $Sr_{0.5}Ca_{0.5}WO_4$.

The WO_4-tetrahedra are isolated from each other and connected by the summits with [Sr/CaO_8] polyhedra as shown in Fig. 3 modeled by visualization for electronic and structural analysis (VESTA) program [33]. The bivalent cations (Ca/Sr) are surrounded by 8 oxygens with the same coordination number. The calcium concentrations in the solid solution $Sr_{1-x}Ca_xWO_4$ ($0 \leq x \leq 1$) create a difference in the electronic environment which influences the optical properties of the material [34].

3.2. Raman spectroscopy analysis

Fig. 4 shows the Raman spectra recorded at room conditions. Raman spectroscopy is considered to be a powerful tool for estimating the degree of structural order-disorder at short-range in oxide materials [35,36].

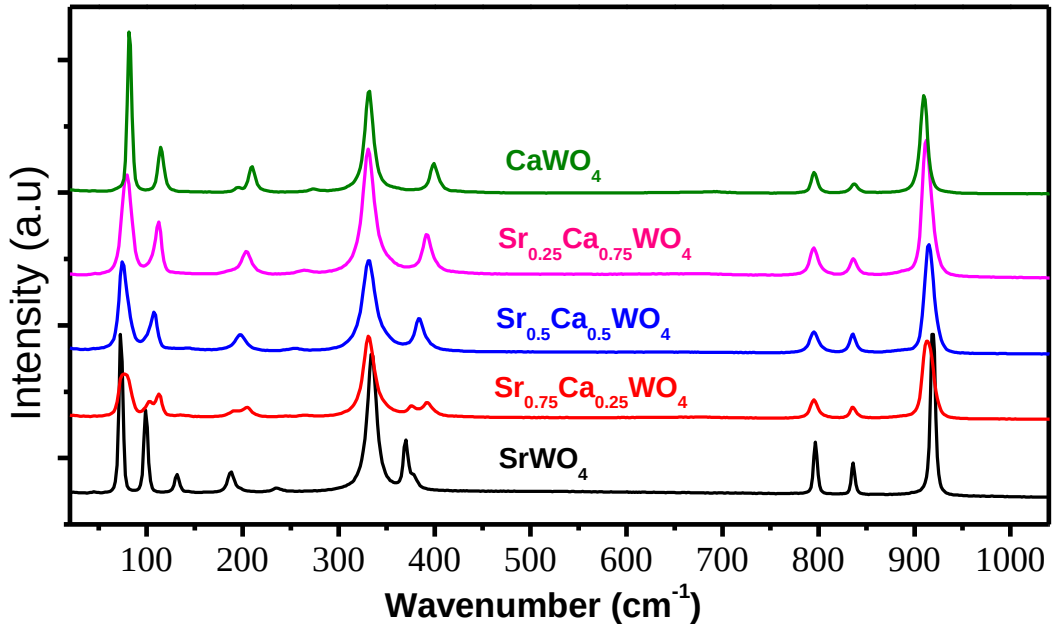

Figure. 4. Raman spectra recorded at room temperature of the scheelite oxide series $Sr_{1-x}Ca_xWO_4$ ($0 \leq x \leq 1$).

For the tetragonal scheelite structure with $I4_1/a$ as space group, (Sr/Ca) and W ions occupy 4a and 4b Wyckoff sites, while the oxygen atoms occupy 16f Wyckoff sites. According to these site occupations, the mode distribution can be decomposed in terms of irreducible representations [37] of the tetragonal system as summarized below, the scheelite-type tetragonal structure exhibit 26 different Raman and infrared vibrational modes.

$$\Gamma_{(I41/a)} = 3A_g + 5A_u + 5B_g + 3B_u + 5E_g + 5E_u$$

$$\Gamma_{(Raman)} = 3A_g + 5B_g + 5E_g$$

$$\Gamma_{(IR)} = 4A_u + 3B_u + 4E_u$$

$$\Gamma_{(acoustic)} = A_u + E_u$$

Table 3. Experimental Raman wavenumbers of $SrWO_4$, $Sr_{0.5}Ca_{0.5}WO_4$, $CaWO_4$.

Mode	$SrWO_4$ (this work)	$CaWO_4$ (this work)	$Sr_{0.5}Ca_{0.5}WO_4$ (this work)	$SrWO_4$ Ref[38]	$SrWO_4$ (15K) Ref[39]	$CaWO_4$ Ref[38]	$CaWO_4$ Ref[40]
T(Bg)	73.12	82.09	75.68	75	74.60	84	84
T(Eg)	99.13	114.81	107.05	101	102.40	117	116
T(Eg)	131.56	194.88	143.8	131	127.90	195	196
T(Bg)		209.62			--	210	212
R(Ag)	187.84	220.10	197.60	187	190.0	218	227
R(Eg)	235.55	273.87	253.80	238	238.5	275	276
υ_2(Ag+Bg)	334.64	331.68	331.62	334	336.7	336	334
υ_4(Bg)	369.73	399.14	383.67	370	372.3	401	402
υ_4(Eg)	377.86	405.58	389.79	378	380.6	409	406
υ_3(Eg)	796.83	795.71	795.40	797	799.5	797	797
υ_3(Bg)	836.03	837.23	835.77	839	839.0	838	838
υ_1(Ag)	919.24	909.81	915.30	925	922.1	912	911

The A and B modes are non-degenerate, while the E modes are doubly degenerate. The subscripts 'g' and 'u' indicate the pairs under inversion in centrosymmetric crystals constrained by the space group $I4_1/a$ in the scheelite structure. Ag, Bg, and Eg Raman modes are the result of the motion of Tetrahedrons $[WO_4]^{2-}$ in the crystal lattice. Therefore, 13 Raman-active vibrational modes of crystals are anticipated, as indicated in irreducible representations. The vibrational modes observed in

Raman spectra for the series $Sr_{1-x}Ca_xWO_4$ are classified into two modes, external and internal modes as reported by Porto et al. for $CaWO_4$ and $SrWO_4$ [38] The external vibration modes are related to lattice phonons (External optical modes) located at wavenumbers below than 210 cm^{-1}, which correspond to polyhedron Sr/CaO_8 vibration in the rigid molecular units. Internal vibrational modes are related to $[WO_4]$ tetrahedral vibrations in the lattice. In the present study, the 13 expected Raman modes in the series $Sr_{1-x}Ca_xWO_4$ was detected. In Table 3 we summarized the Raman active frequencies for $SrWO_4$, $Sr_{0.5}Ca_{0.5}WO_4$, and $CaWO_4$ as an example and the Raman motion from the refs [38-40] are given for comparison.

3.2. Optical properties: UV-visible and bandgap study

The optical absorption study is very useful as a technique to understand the basic analysis of optical behavior. Indeed, the optical band gap can be found in the following equation:

$$(\alpha h\nu)^{m} = A(h\nu - E_g)$$

A is a constant depending on the transition probability, and *m* is equal to 2 for a direct gap and 1/2 for an indirect gap. To calculate the bandgap energies, we plot $(\alpha h\nu)^{m}$ Versus the incident radiation energy ($h\nu$). By extrapolating the values of the absorption coefficient α to zero, we can find the band gap values [24].

According to the theoretical investigation below, the band structures show that the bandgap is direct for all the samples. Thus *m* will take *2*, and the optical band gap will be found in the plot of $(\alpha h\nu)^2$ versus ($h\nu$). Fig. 5 shows the experimental optical band gap study of $Sr_{1-x}Ca_xWO_4$ ($0 \le x \le 1$) compounds.

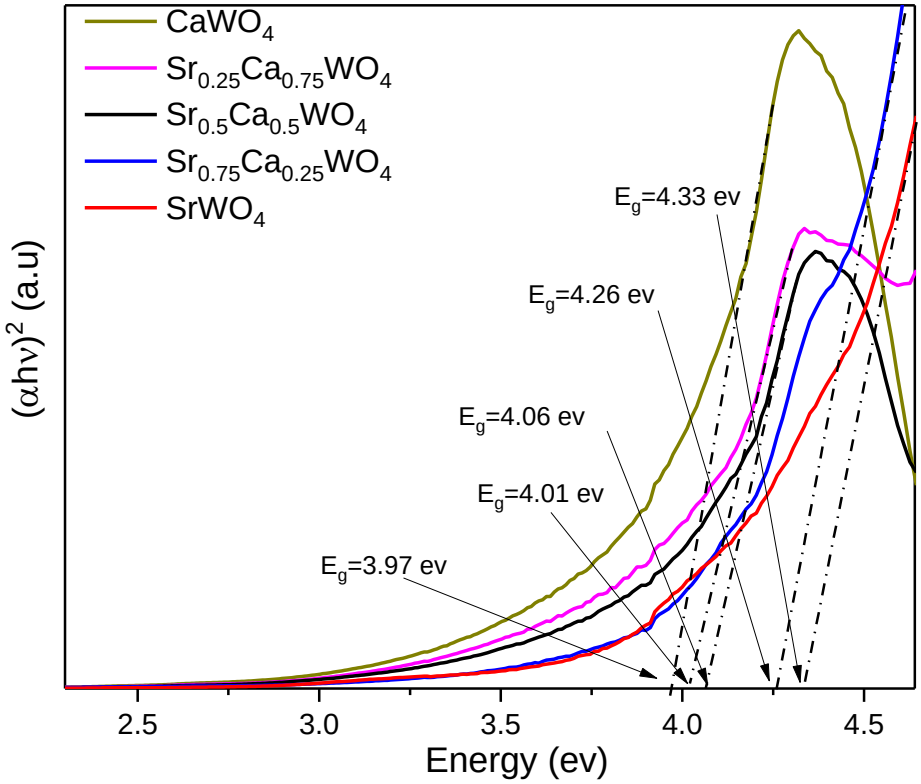

Figure. 5. Plot of $(\alpha h\nu)^2$ versus ($h\nu$) for the estimation of the bandgap energy, direct gap of $Sr_{1-x}Ca_xWO_4$ ($0 \le x \le 1$) with experimental data.

3.3. Theoretical investigation

3.3.1. Band Structure

The bandgap can be related to a lot of factors, such as preparation method, shape (thin film or powder), particle morphology, heat treatment temperature and processing time [41]. We also believe that the calculated values of bandgap depend on the type of approximation used. So in order to determine the value and the type of bandgap in $Sr_{1-x}Ca_xWO_4$ samples.

We have calculated the band structure of such compound using the very popular and quite successful GGA approximation (see Fig. 6**)**. This Figure shows that the minimum of the conduction band and the maximum of the valence band are at the same point 'Γ'. This indicates that the gap of all compositions of $Sr_{1-x}Ca_xWO_4$ is direct.

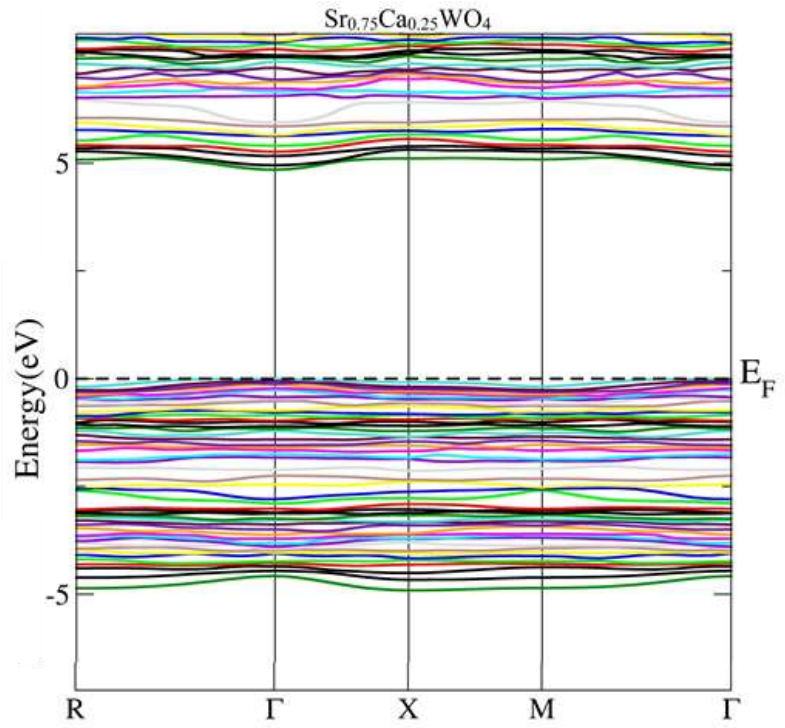
$Sr_{0.75}Ca_{0.25}WO_4$
Energy(eV)
5
0
-5
E_F
R
Γ
X
M
Γ

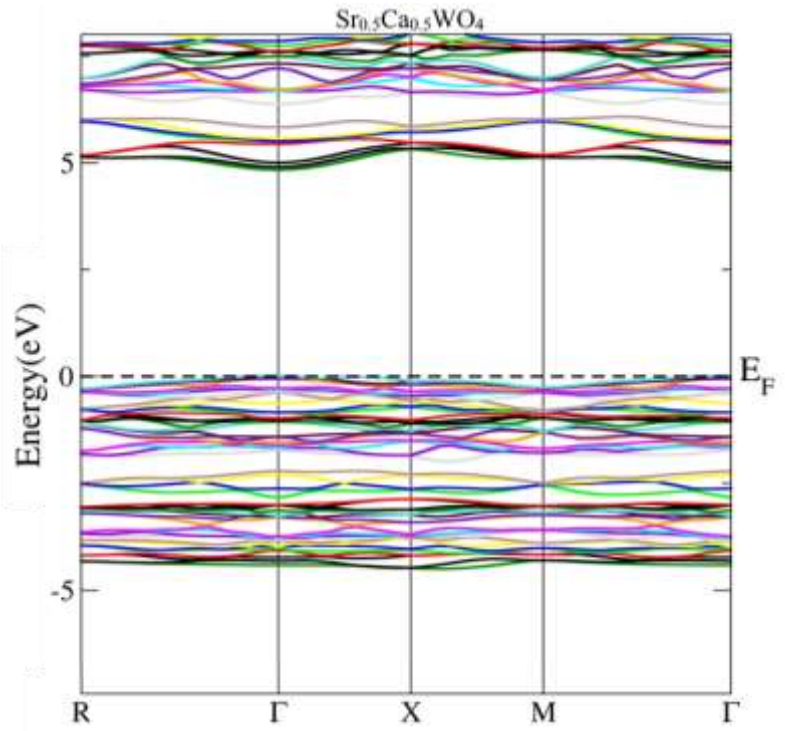
$Sr_{0.5}Ca_{0.5}WO_4$
Energy(eV)
5
0
-5
E_F
R
Γ
X
M
Γ

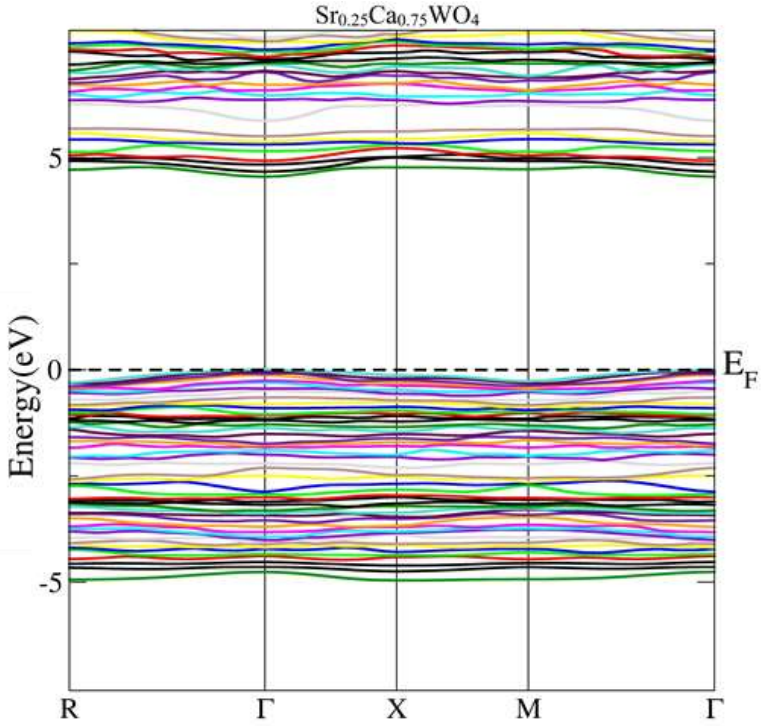

Figure. 6. Calculated GGA band structure of $Sr_{1-x}Ca_xWO_4$ (x=0.25; 0.5; 0.75)

3.3.2. Total /Partial density of states

Fig.. 7(a, b, c) shows the total and the partial density of state of $Sr_{1-x}Ca_xWO_4$ (x=0.25, 0.5, 0.75), we proceed this calculation in order to understand the electronic configuration of this material. The total density of state shows the existence of different bands in different regions. The PDOS calculations indicate that in $Sr_{1-x}Ca_xWO_4$. The valence band VB is mainly formed by p-orbitals of oxygen O^{2-} with a minimal contribution from the tungsten W^{6+} d-states. The conduction band CB, however, is formed mainly from the tungsten d-states with small contributions from p-states of oxygen. The *s* and *p*-states of Sr^{2+} contribute in the TDOS by an occurrence of a peak which appears at E=-13 eV from the main VB, and the region from -17 eV to -15.68 eV is mainly due to the *s* and *p*-states of Ca^{2+}.

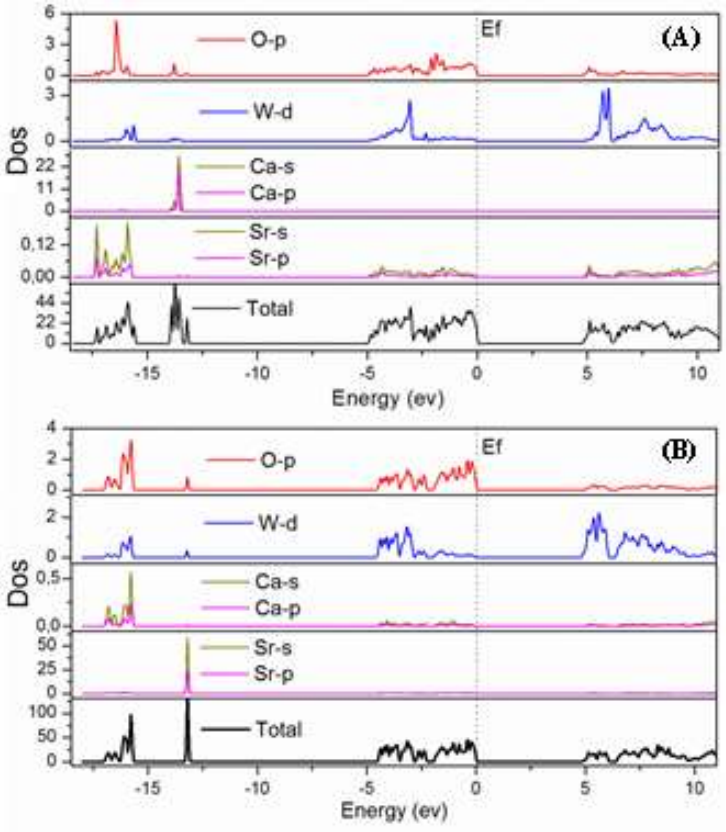

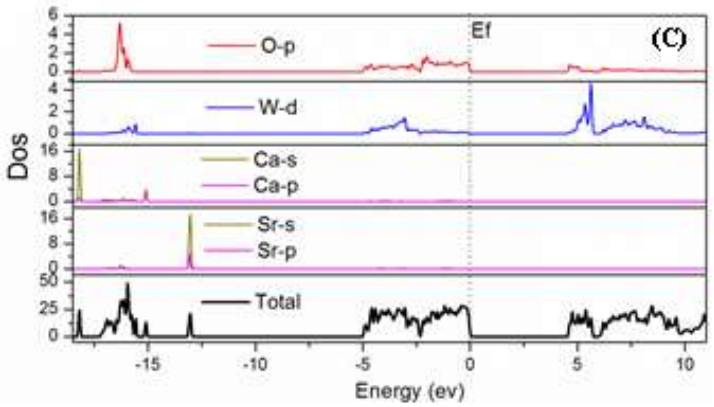

Figure 7. Calculated density of states and PDOS of constituent atoms in $Sr_{0.75}Ca_{0.25}WO_4$ (A) $Sr_{0.5}Ca_{0.5}WO_4$ (B) $Sr_{0.25}Ca_{0.75}WO_4$ (C)

3.3.3. Optical properties: Calculated absorption spectra

According to Fig. 7 the energy difference between the top of the valence band and the bottom of the conduction band corresponds to a charge transfer between the p states of oxygen O^{2-} and the tungsten W^{6+} d-states, these states explain the origin of the bandgap. Fig. 8 shows the Absorption spectra versus the energy of $Sr_{1-x}Ca_xWO_4$ ($0 \leq x \leq 1$) compounds with the first principle calculations.

Fig. 9 shows that the direct bandgap energies derived from the calculated absorption spectra and the one measured by UV-visible much with each other. It was found that the direct band-gap energy decreases as 'Ca' content in the composition increases which means that the bandgap energy of $CaWO_4$ is lower than one of $SrWO_4$ which is correlated with the decreases of the lattice parameters as shown in the inset. This decrease in the lattice parameters is also accompanied by an increase in the W–O bond lengths (Table 2). Resulting in a lowering of the binding forces between the valence electrons of the oxygen O^{2-} and the tungsten W^{6+}. As a consequence, the band-gap energy decreases.

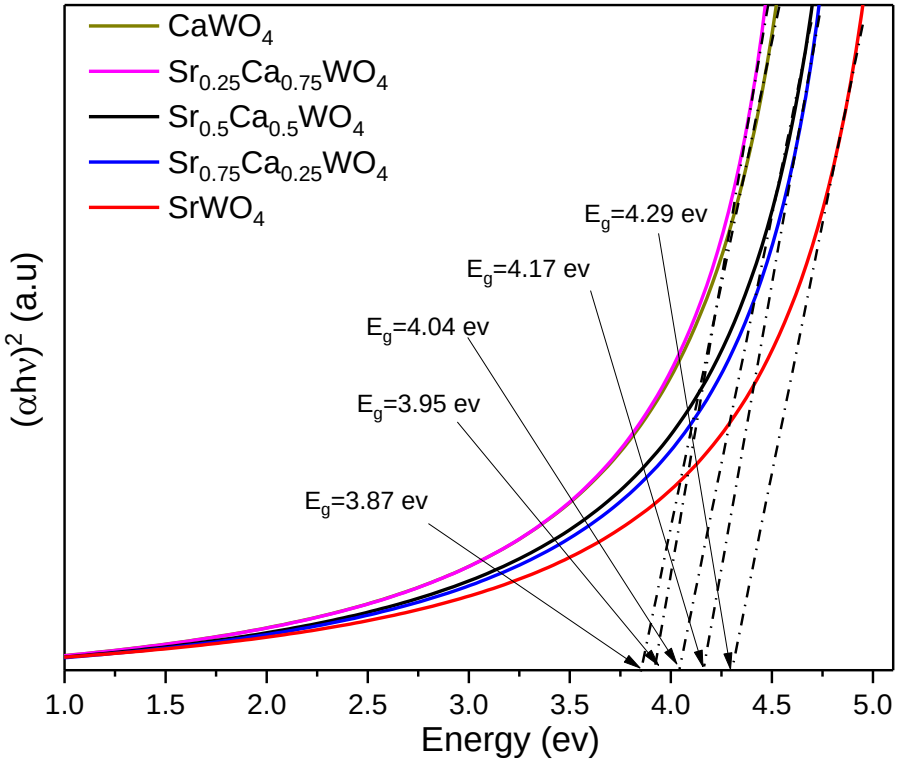

Figure. 8. Plot of $(\alpha h\nu)^2$ versus $(h\nu)$ for the estimation of the bandgap energy, direct gap of $Sr_{1-x}Ca_xWO_4$ ($0 \leq x \leq 1$) with first calculations.

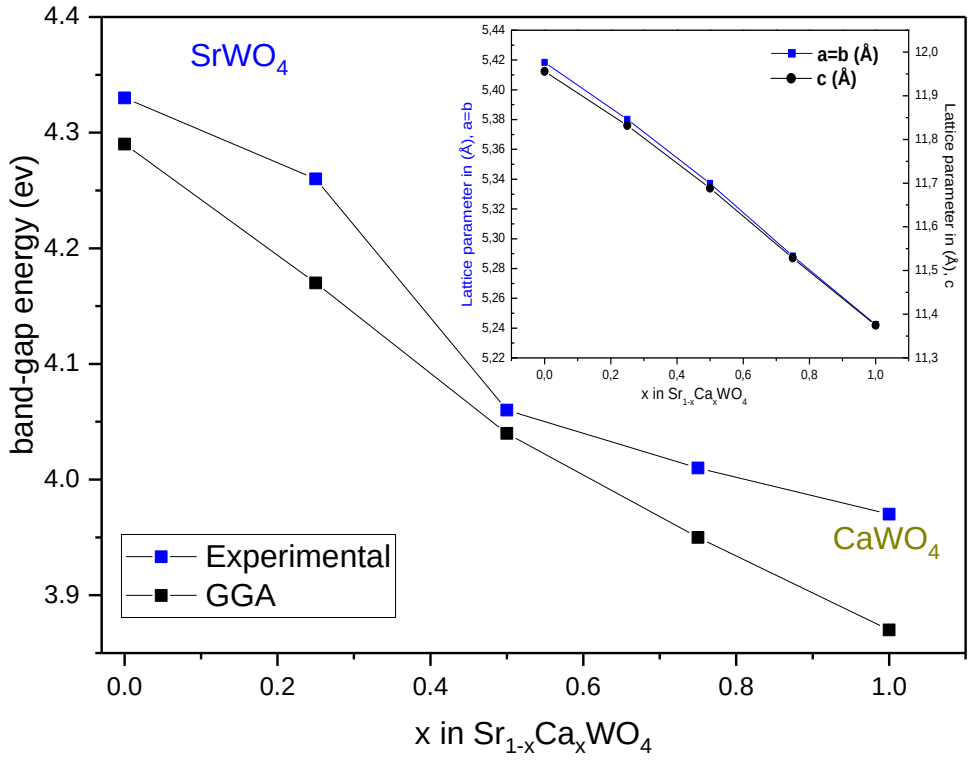

Figure. 9. The variation of the theoretical and experimental optical band gap of $Sr_{1-x}Ca_xWO_4$ as a function of Ca content. The Inset illustrates the variation of the lattice parameters

4. Conclusion

Strontium Calcium Tungstate $Sr_{1-x}Ca_xWO_4$ ($0 \leq x \leq 1$) solid solution was prepared with success by solid-state reaction method. Rietveld refinements showed that the samples crystallized in a tetragonal body-centred symmetry, space group *I*41/*a*. A decrease in the lattice parameters as a function of the increase of (x) in the lattice was observed. A variation of the atomic positions related to oxygen atoms was also observed and causes changes in Sr/Ba–O and W–O bond lengths.

First-principles calculations based on FP-LAPW method with generalized gradient approximation (GGA) was used to calculate the electronic and optical properties of $Sr_{1-x}Ca_xWO_4$ insulators ($E_g > 3eV$). The theoretical and the experimental studies show that the substitution of Sr^{2+} by Ca^{2+} ions promote a decrease in optical direct bandgap values due to the appearance of intermediary energy levels within the bandgap which is also proportional to the decrease of the de interatomic distance between oxygen O^{2-} and the tungsten W^{6+}.

References

1- D. Rangappa, T. Fujiwara, T. Watanabe, M. Yoshimura, Preparation of Ba1−xSrxWO4 and Ba1−xCaxWO4 films on tungsten plate by mechanically assisted solution reaction at room temperature, Materials Chemistry and Physics. **2008**,109,217–223.

2- R. Lacomba-Perales, J. Ruiz-Fuertes, D. Errandonea, D. Martínez-García, A. Segura, Optical absorption of divalent metal tungstates: Correlation between the band-gap energy and the cation ionic radius, EPL Europhysics Letters). **2008**,83,37002.

3- S.D. Colson, K.N. Wong, Overtone spectra of crystalline CaWO4: vibrational exciton density-of-states functions, Chemical Physics. **1982**, 69,223–228.

4- M. Ait Haddouch, Y. Aharbil, Y. Tamraoui, B. Manoun, P. Lazor, S. Benmokhtar, Synthesis, X-ray diffraction, Raman spectroscopy and Electronic structure studies of (Ba1-xSrx)WO4 ceramics, Journal of Materials and Environmental Science. **2015**,6.

5- M.V. Nazarov, B.S. Tsukerblat, E.-J. Popovici, D.Y. Jeon, Optical lines in europium–terbium double activated calcium tungstate phosphor, Physics Letters A. **2004**,330,291–298.

6- Z. Wang, J.J. Bian, Low-temperature sintering and microwave dielectric properties of Ba3(PO4)2–BaWO4 composite ceramics, Ceramics International. **2014**,40,8507–8511.

7- H. Zhuang, Z. Yue, S. Meng, F. Zhao, L. Li, Low-Temperature Sintering and Microwave Dielectric Properties of Ba3(VO 4)2-BaWO4 Ceramic Composites, Journal of the American Ceramic Society. **2008**,91,3738–3741.

8- K. V. Terebilenko, K.L. Bychkov, K.E. Klymyshyna, V.N. Baumer, M.S. Slobodyanik, E. V. Khomenko, V.P. Dotsenko, Single Crystals of KRE(MoO4) 2, (RE- Ce, Pr) Obtained from Fluorides: Scheelite-Related Structure and

Luminescence, Crystal Research and Technology. **2017**,52,1700222.
9- R.C. Lima, M. Anicete-Santos, E. Orhan, M.A.M.A. Maurera, A.G. Souza, P.S. Pizani, E.R. Leite, J.A. Varela, E. Longo, Photoluminescent property of mechanically milled BaWO4 powder, Journal of Luminescence. **2007**,126,741–746.
10- F.M. Pontes, M.A.M.A. Maurera, A.G. Souza, E. Longo, E.R. Leite, R. Magnani, M.A.C. Machado, P.S. Pizani, J.A. Varela, Preparation, structural and optical characterization of BaWO4 and PbWO4 thin films prepared by a chemical route, Journal of the European Ceramic Society. **2003**,23,3001–3007.
11- P. Afanasiev, Molten salt synthesis of barium molybdate and tungstate microcrystals, Materials Letters. **2007**,61,4622–4626.
12- Q. Guo, O.J. Kleppa, Note on the enthalpies of formation of SrWO4 and BaWO4 determined by high-temperature direct synthesis calorimetry from SrCO3 + WO3 and BaCO3 + WO3, Thermochimica Acta. **1997**,303,183–186.
13- N. Khobragade, E. Sinha, S.K. Rout, M. Kar, Structural, optical and microwave dielectric properties of Sr1−xCaxWO4 ceramics prepared by the solid-state reaction route, Ceramics International. **2013**, 39, 9627–9635.
14- C.S. Lim, Solid-state metathetic synthesis of BaMO4 (M = W, Mo) assisted by microwave irradiation, Journal of Ceramic Processing Research. **2011**, 12, 544–548.
15- Q. Guo, O.J. Kleppa, Enthalpies of formation from the component oxides of MgWO4, CaWO4 (scheelite), SrWO4, and BaWO4, determined by high-temperature direct synthesis calorimetry, Thermochimica Acta. 1996, 288, 53–61.
16- S.K. Arora, B. Chudasama, Crystallization and optical properties of CaWO4 and SrWO4, Crystal Research and Technology. **2006**, 41, 1089–1095.
17- P. Hohenberg, W. Kohn, Inhomogeneous Electron Gas, Physical Review. **1964**, 136, B864–B871.
18- J. Rodriguez-Carvajal, FULLPROF 2000: A Rietveld Refinement and Pattern Matching Analysis Program, **2008**.
19- T. Roisnel, J. Rodríquez-Carvajal, WinPLOTR: A Windows Tool for Powder Diffraction Pattern Analysis, Materials Science Forum. **2001**, 378–381, 118–123.
20- M. Azdouz, B. Manoun, M. Azrour, L. Bih, L. El Ammari, S. Benmokhtar, P. Lazor, Synthesis, Rietveld refinements and Raman spectroscopy studies of the solid solution Na1−xKxPb4(VO4)3 (0⩽x⩽1), Journal of Molecular Structure. **2010**, 963, 258–266.
21- Y. Tamraoui, B. Manoun, F. Mirinioui, I. Saadoune, R. Haloui, A. Elhachmi, E. Saad, P. Lazor, Temperature and composition induced phase transitions in Sr2−xCa1+xTeO6 ($0 \leq x \leq 2$) double perovskite oxides, Journal of Molecular Structure. **2017**, 1131.
22- R.A. May, K.J. Stevenson, Software Review of Origin 8, Journal of the American Chemical Society. **2009**, 131, 872.
23- P. Kubelka, F. Munk, An Article on Optics of Paint Layers (engl. Übersetzung), Z. Tech. Phys. **1931**, 12, 593–601.
24- J. Tauc, Optical properties and electronic structure of amorphous Ge and Si, Materials Research Bulletin. **1968**, 3, 37–46.
25- P. Blaha, K. Schwarz, G.K.H. Madsen, D. Kvasnicka, J. Luitz, Computer code WIEN2K, Vienna University of Technology. **2001**.
26- J.P. Perdew, K. Burke, M. Ernzerhof, Generalized Gradient Approximation Made Simple, Physical Review Letters. **1996**, 77, 3865–3868.
27- A. Boultif, D. Loueer, D. Louër, Indexing of powder diffraction patterns for low-symmetry lattices by the successive dichotomy method, Journal of Applied Crystallography. **1991**, 24, 987–993.
28- R.D. Shannon, Revised effective ionic radii and systematic studies of interatomic distances in halides and chalcogenides, Acta Crystallographica Section A. **1976**, 32, 751–767.
29- A. Priya, E. Sinha, S.K. Rout, Structural, optical and microwave dielectric properties of Ba1−xSrxWO4 ceramics prepared by solid-state reaction route, Solid State Sciences. **2013**, 20, 40–45.
30- I.C. Nogueira, L.S. Cavalcante, P.F.S. Pereira, M.M. De Jesus, J.M. Rivas Mercury, N.C. Batista, M.S. Li, E. Longo, Rietveld refinement, morphology and optical properties of (Ba1-xSrx)MoO4 crystals, Journal of Applied Crystallography. **2013**, 46, 1434–1446.
31- S.K. Ghosh, S.K. Rout, A. Tiwari, P. Yadav, J.C. Sczancoski, M.G.R. Filho, L.S. Cavalcante, Structural refinement, Raman spectroscopy, optical and electrical properties of (Ba1−xSrx)MoO4 ceramics, Journal of Materials Science: Materials in Electronics. **2015**, 26, 8319–8335.
32- M.E. Fleet, Distortion parameters for coordination polyhedra, Mineralogical Magazine. **1976**, 40, 531–3.
33- K. Momma, F. Izumi, IUCr, VESTA: a three-dimensional visualization system for electronic and structural analysis, Journal of Applied Crystallography. **2008**, 41, 653–658.
34- R.F. Gonçalves, L.S. Cavalcante, I.C. Nogueira, E. Longo, M.J. Godinho, J.C. Sczancoski, V.R. Mastelaro, I.M. Pinatti, I.L. V. Rosa, A.P.A. Marques, Rietveld refinement, cluster modelling, growth mechanism and photoluminescence properties of CaWO4:Eu3+ microcrystals, CrystEngComm. **2015**, 17, 1654–1666.
35- S.K. Ghosh, M. Ganguly, S.K. Rout, T.P. Sinha, Order-disorder correlation on the local structure and photo-electrical properties of La3+ ion modified BZT ceramics, The European Physical Journal Plus. **2015**, 130, 68.

36- L.P. Lyashenko, L.G. Shcherbakova, I.I. Tartakovskii, A.A. Maksimov, R.D. Svetogorov, Y. V. Zubavichus, Order-Disorder Structural Transformations in Nanocrystalline Highly Imperfect Gd2MO5 (M = Zr and Hf) Fluorite Derivatives, Inorganic Materials. **2018**, 54, 245–252.
37- M.I. Aroyo, J.M. Perez-Mato, C. Capillas, E. Kroumova, S. Ivantchev, G. Madariaga, A. Kirov, H. Wondratschek, Bilbao Crystallographic Server: I. Databases and crystallographic computing programs, Zeitschrift Für Kristallographie - Crystalline Materials. **2006**, 221.
38- S.P.S. Porto, J.F. Scott, Raman Spectra of CaWO4, SrWO4, CaMoO4, and SrMoO4, Physical Review. **1967**, 157, 716–719.
39- J. Suda, P.G. Zverev, Investigation of bandgap effect and dephasing on Raman line broadening for the highest-frequency Ag mode in comparison with SrWO4 and SrMoO4, Vibrational Spectroscopy. **2016**, 84, 127–132.
40- D. Christofilos, S. Ves, G.A. Kourouklis, Pressure-induced phase transitions in alkaline earth tungstates, Physica Status Solidi (B) Basic Research. **1996**, 198, 539–544. d.
41- B. Coluzzi, A. Biscarini, G. Mazzolai, F.M. Mazzolai, A. Tuissi, Effect of H-Doping on Damping Capacity of Various NiTi-Based Alloys at kHz Frequencies, Journal of Engineering Materials and Technology. **2006**, 128, 254.